Supporting Information

Frequency and Temperature Dependent Dielectric Properties of $CoFe_{2-x}Y_xO_4$: Polarization and Conduction Mechanisms Pertained to Crystallographic Symmetry and Electronic Transitions

Arun Raj R S[1], Aruna Joseph[1], Shamima Hussain[2], Mohd Fahad[3], Tuhin Maity[4], P M Sarun[3] and Lija K Joy[1, *]

[1] Centre for Advanced Functional Materials (CAFM), Department of Physics, Bishop Moore College, Mavelikara, Alappuzha, Kerala, 690110, India
[2] UGC-DAE Consortium for Scientific Research, Kalpakkam Node, Kokilamedu-603104, India
[3] Functional Ceramics Laboratory, Department of Physics, Indian Institute of Technology (Indian School of Mines), Dhanbad, 826004, India
[4] School of Physics, Indian Institute of Science Education and Research, Thiruvananthapuram, Kerala 695551, India
[*] Corresponding author email: - lijakjoy@gmail.com

3. Results and Discussions

3.1 Structural and Compositional Studies

3.1.2 FTIR studies

Table S1. Vibrational bands of $CoFe_{2-x}Y_xO_4$ (x = 0.00, 0.02, 0.04, 0.08)

Composition	ν_t (cm^{-1})	ν_o (cm^{-2})
0.00	536.16	289.16
0.02	541.84	306.64
0.04	546.00	315.93
0.06	550.14	329.92
0.08	552.49	335.86
0.10	549.25	330.15

3.1.3 XPS Studies

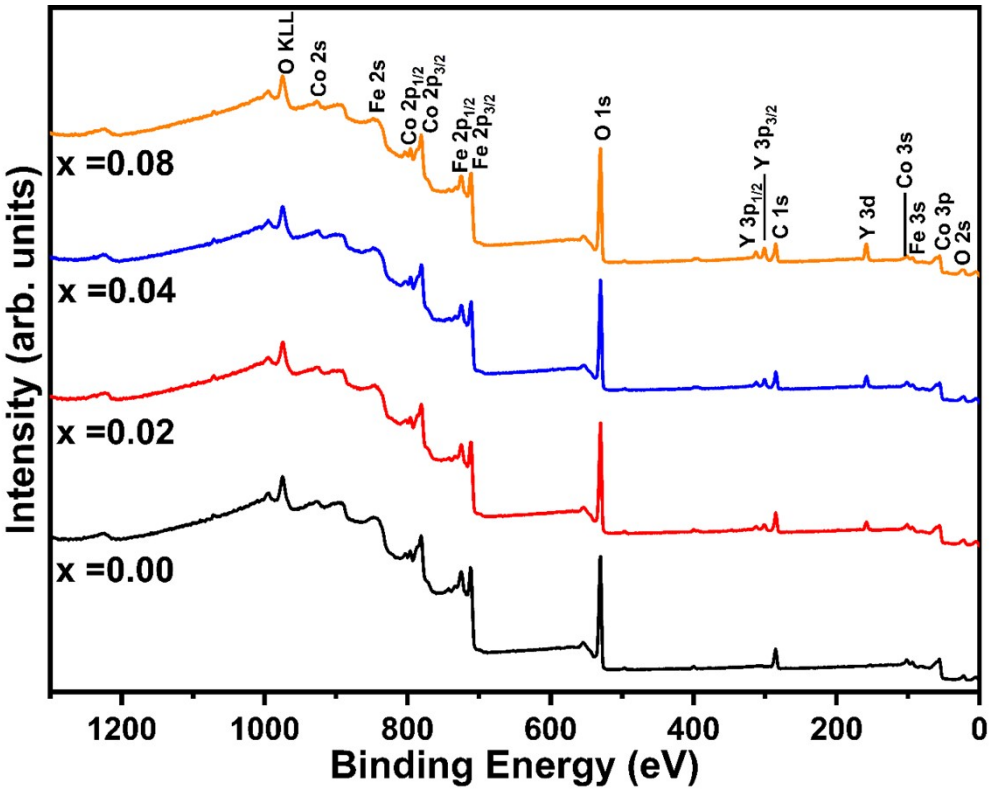

Figure S1. Wide scan survey spectrum of $CoFe_{2-x}Y_xO_4$ (x = 0.00, 0.02, 0.04, 0.08) at room temperature.

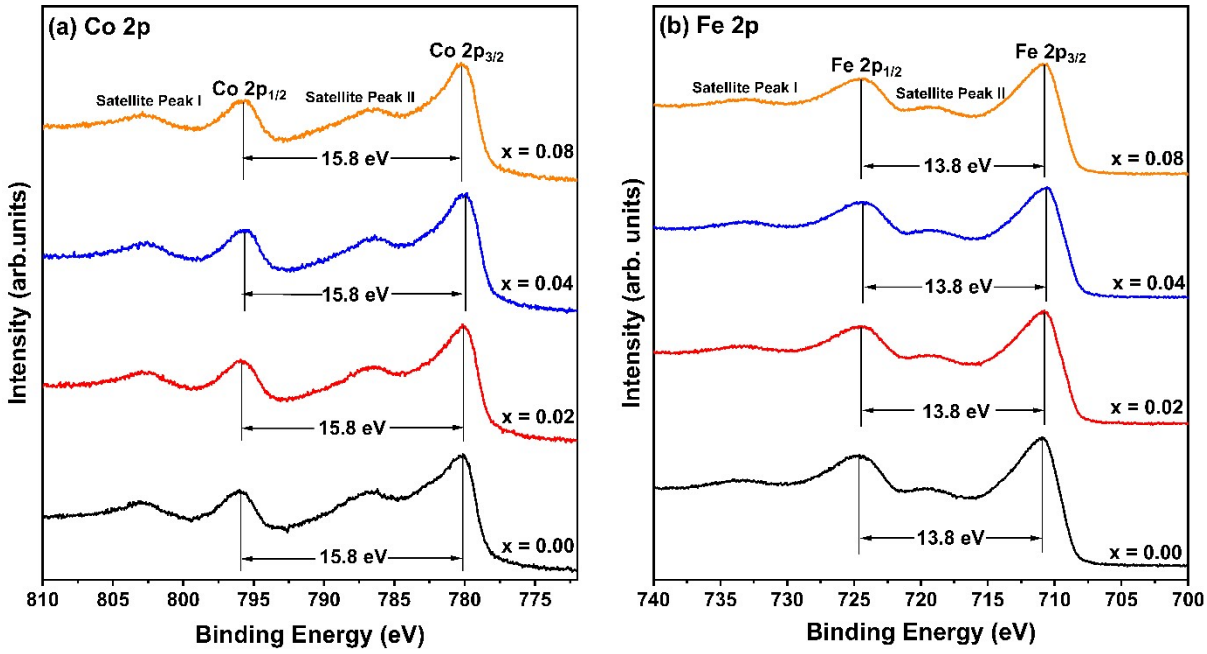

Figure S2. (a) Co 2p core level XPS spectra and (b) Fe 2p core level XPS spectra of $CoFe_{2-x}Y_xO_4$ (x = 0.00, 0.02, 0.04, 0.08)

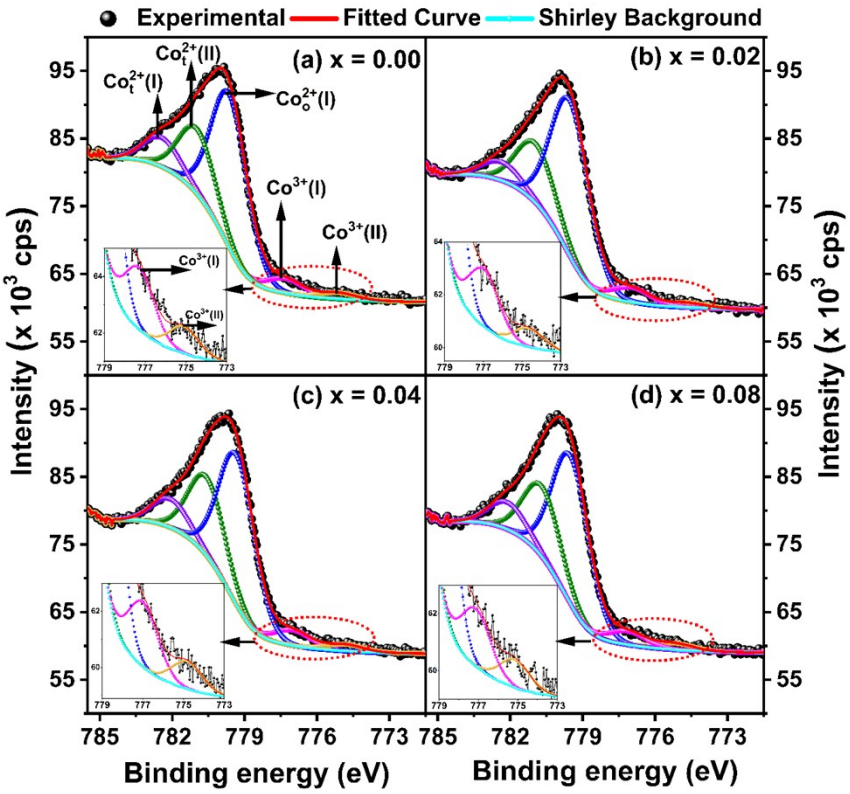

Figure S3. Deconvoluted Co $2p_{3/2}$ XPS spectra of $CoFe_{2-x}Y_xO_4$ (x = 0.00, 0.02, 0.04 and 0.08). The inset shows the magnified image of Co^{3+} (I) and Co^{3+} (II) peaks in $CoFe_{2-x}Y_xO_4$.

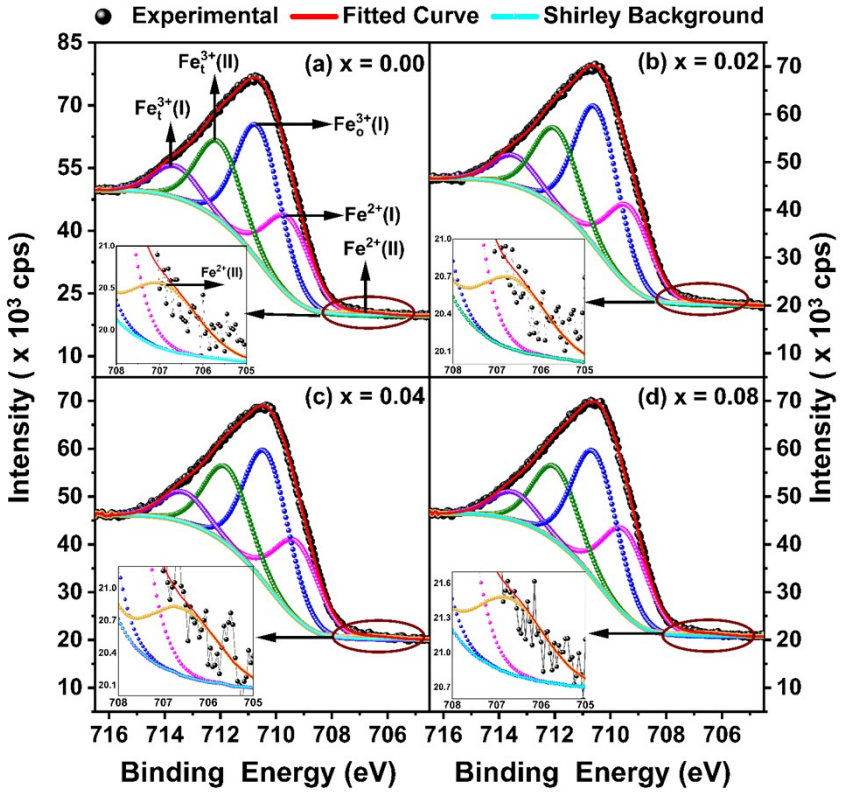

Figure S4. Deconvoluted Fe $2p_{3/2}$ XPS spectra of $CoFe_{2-x}Y_xO_4$ (x = 0.00, 0.02, 0.04 and 0.08). The inset shows a magnified image of the Fe^{2+} (II) peak in $CoFe_{2-x}Y_xO_4$.

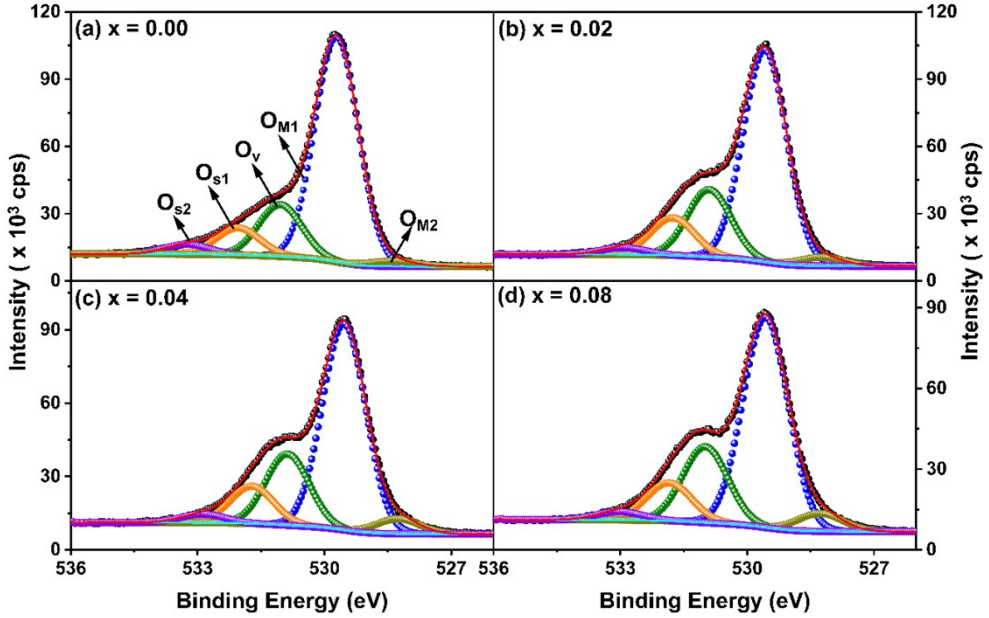

Figure S5. Deconvoluted O1s XPS spectra of $CoFe_{2-x}Y_xO_4$ (x = 0.00, 0.02, 0.04 and 0.08).

Table S2: (a) Binding energy of Co, Fe, and Y in $CoFe_{2-x}Y_xO_4$ (x = 0.00, 0.02, 0.04, and 0.08) system.

Binding Energy in eV					
Spectrum	**Assignment**	**Composition**			
		x = 0.00	**x = 0.02**	**x = 0.04**	**x = 0.08**
Co $2p_{3/2}$	$Co^{2+}_t\ (I)$	782.43	782.37	782.06	782.11
	$Co^{2+}_t\ (II)$	780.97	780.95	780.57	780.69
	$Co^{2+}_o\ (I)$	779.62	779.52	779.32	779.50
	$Co^{3+}\ (I)$	777.31	776.99	777.00	777.15
	$Co^{3+}\ (II)$	775.11	774.66	774.83	775.17
Fe $2p_{3/2}$	$Fe^{3+}_t\ (I)$	713.60	713.46	713.30	713.48
	$Fe^{3+}_t\ (II)$	712.04	711.94	711.77	711.97
	$Fe^{3+}_o\ (II)$	710.62	710.49	710.34	710.54
	$Fe^{2+}\ (I)$	709.55	709.33	709.24	709.48
	$Fe^{2+}\ (II)$	706.92	706.66	706.58	706.72
Y $3d_{3/2}$	Y^{3+}_o	--	159.37	159.28	159.63
	Y^{3+}_{ov}	--	--	--	158.58
Y $3d_{5/2}$	Y^{3+}_o	--	157.29	157.21	157.58
	Y^{3+}_{ov}	--	--	--	156.45
O 1s	O	533.25	532.93	532.87	533.02
	O_s	532.04	531.75	531.71	531.84
	O_v	531.04	530.90	530.87	530.99

	O_{M1}	529.71	529.58	529.53	529.56
	O_{M2}	528.37	528.24	528.25	528.27

3.1.4 EDS Analysis

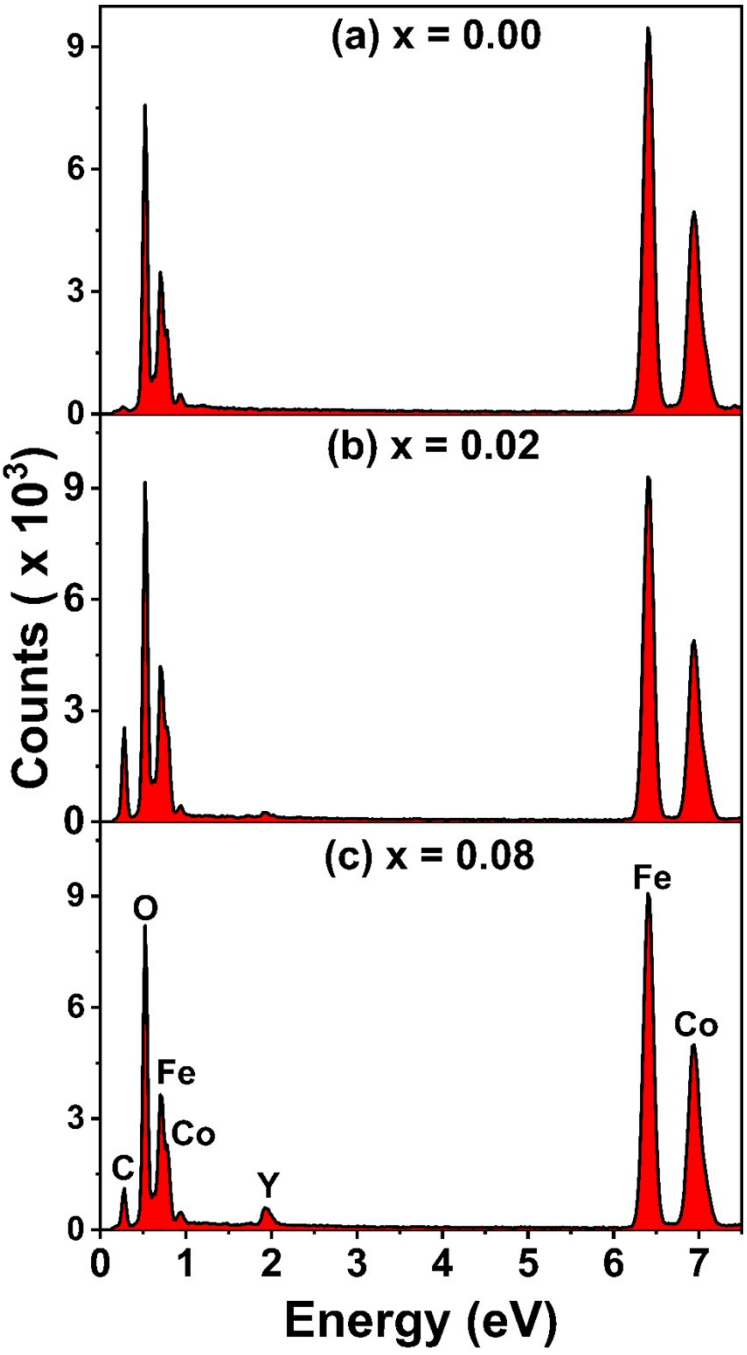

Figure S6. EDS micrographs of $CoFe_{2-x}Y_xO_4$ (x = 0.00, 0.02 and 0.08)

Table S3. The atomic ratio of Co/Fe and Y/Fe in $CoFe_{2-x}Y_xO_4$ (x = 0.00, 0.02 and 0.08).

Composition	Co/Fe ratio		Y/Fe ratio	
	From EDS	Theoretical	From EDS	Theoretical
0.00	0.55	0.5	0	0
0.02	0.53	0.51	0.01	0.01

0.08	**0.58**	**0.52**	**0.03**	**0.04**

3.2 Morphological studies

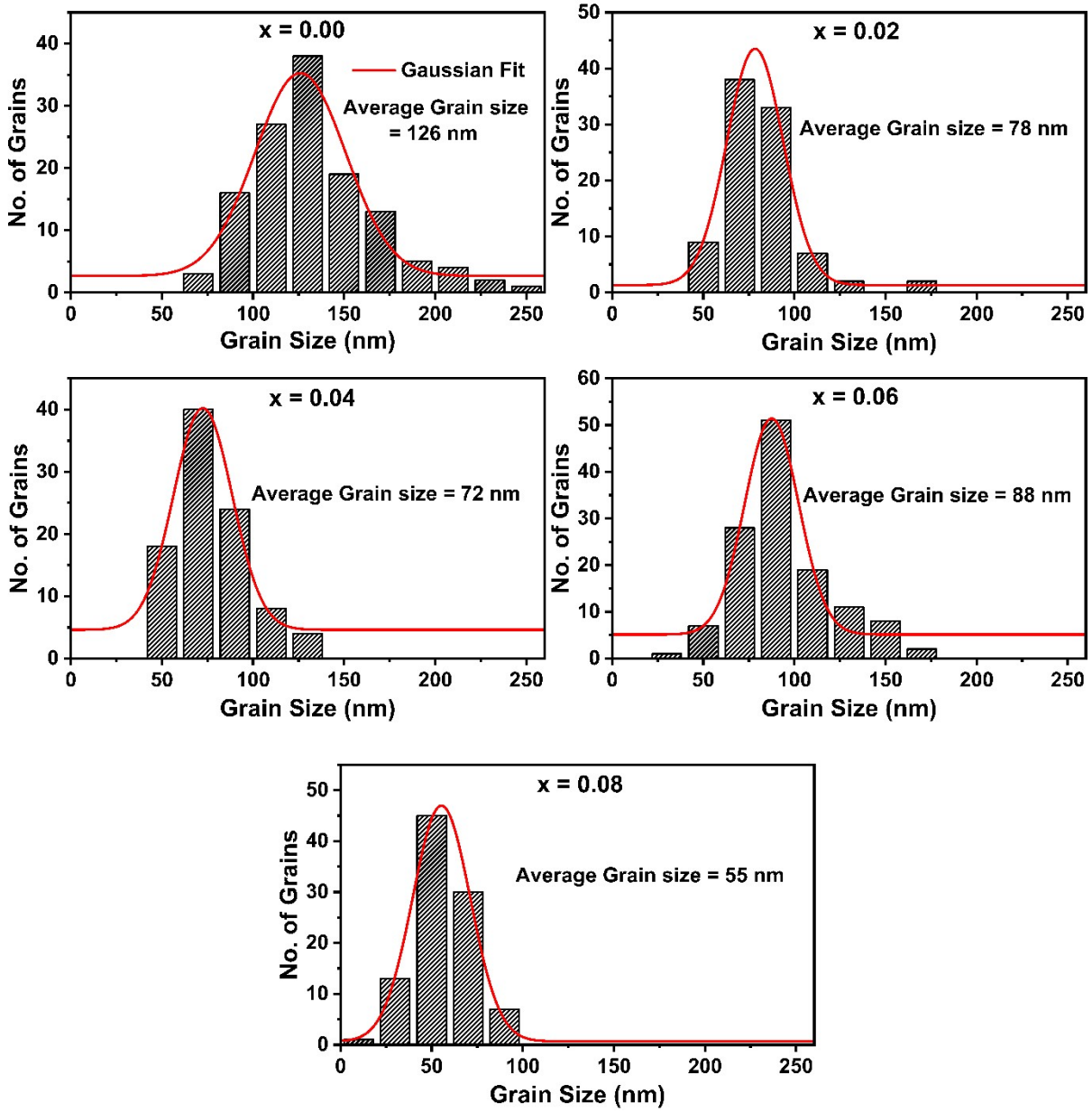

Figure S7 Grain distribution curves of $CoFe_{2-x}Y_xO_4$ (x = 0.00, 0.02, 0.04, 0.06, and 0.08)

3.3 Optical Studies

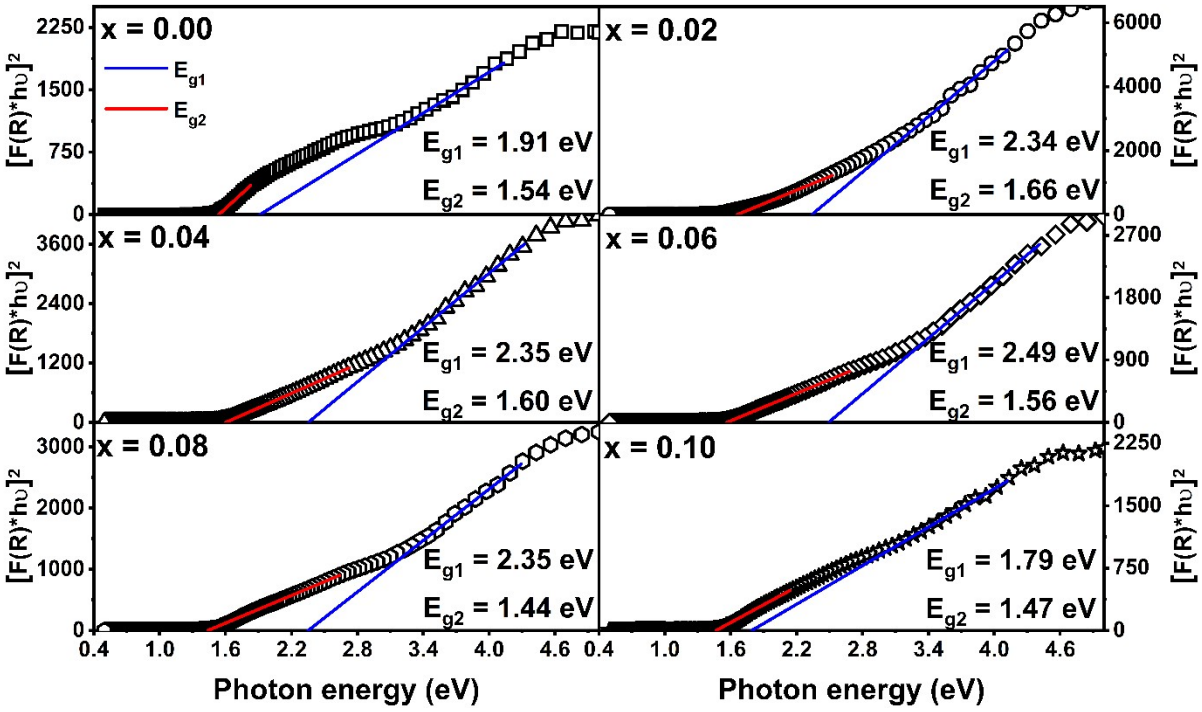

Figure S8. Direct band gap calculation of $CoFe_{2-x}Y_xO_4$ (x = 0.00, 0.02, 0.04, 0.06, 0.08 and 0.10)

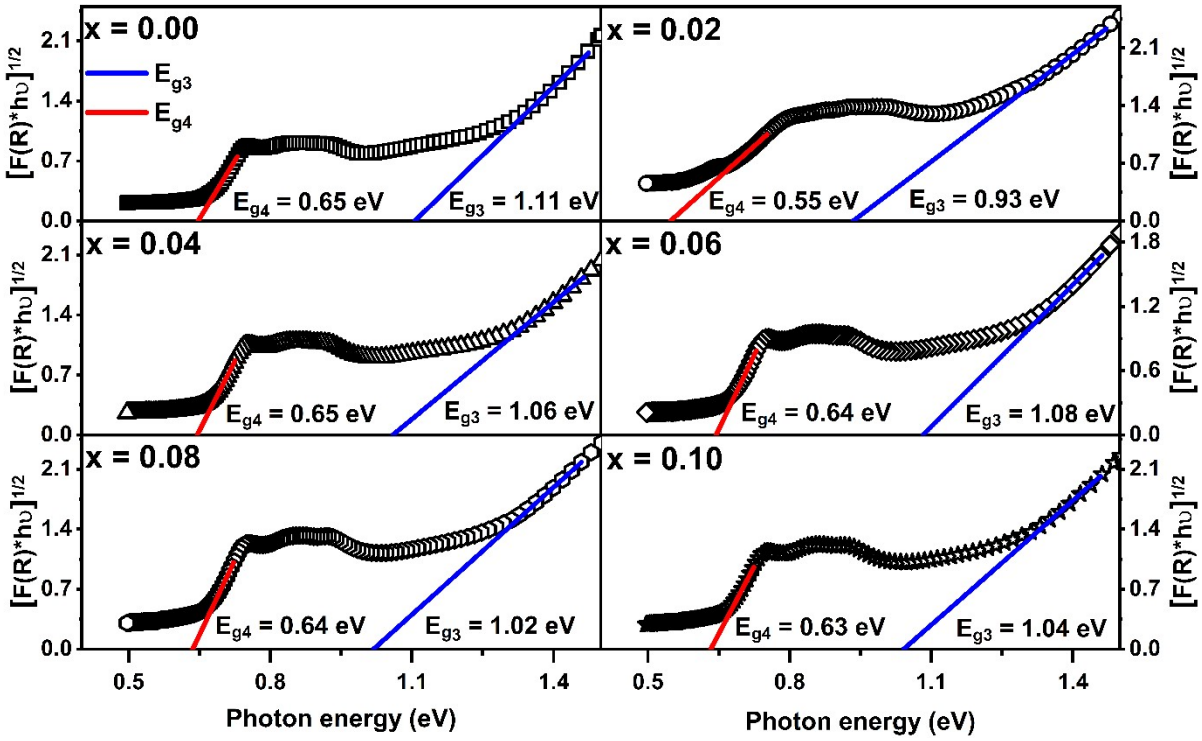

Figure S9. Indirect band gap calculation of $CoFe_{2-x}Y_xO_4$ (x = 0.00, 0.02, 0.04, 0.06, 0.08 and 0.10)

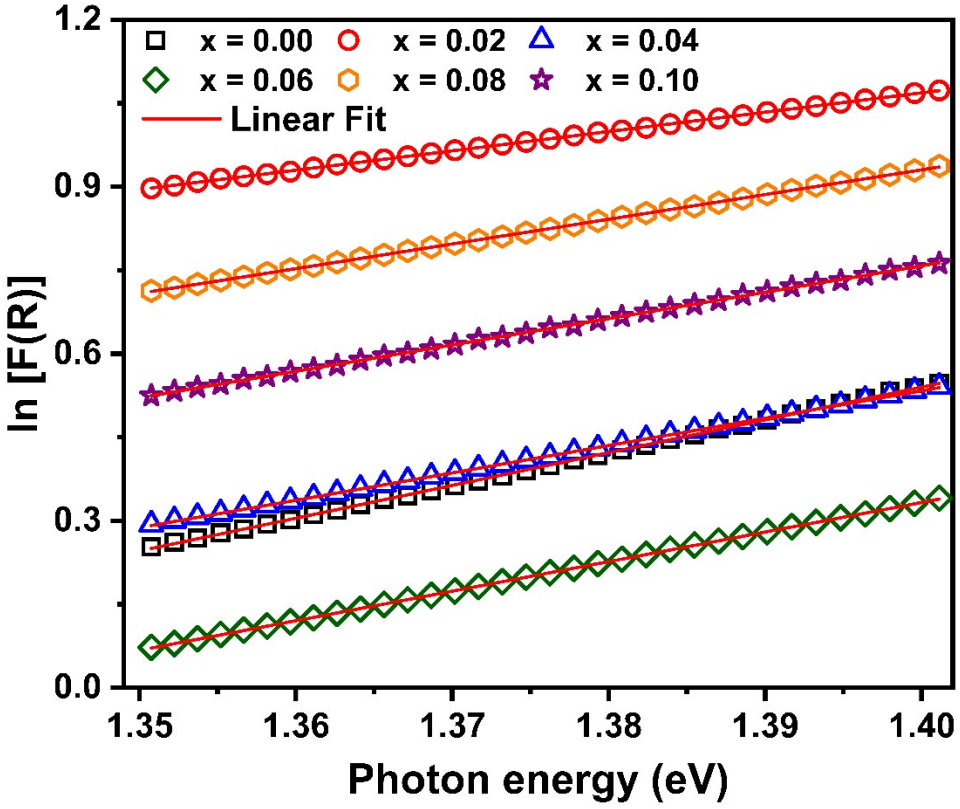

Figure S10. Estimation of Urbach energy of $CoFe_{2-x}Y_xO_4$ (x = 0.00, 0.02, 0.04, 0.06, 0.08 and 0.10)

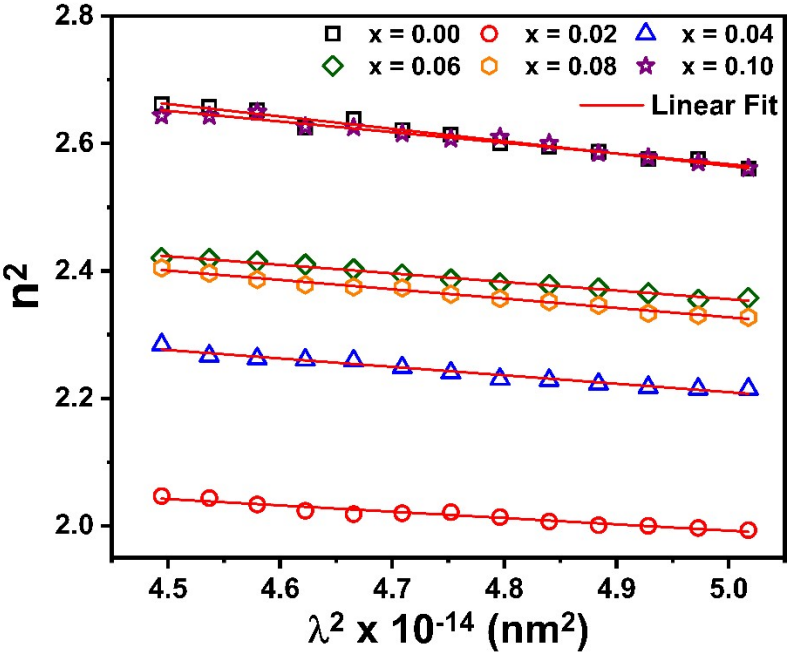

Figure S11. Estimation of ε_L and N/m* of $CoFe_{2-x}Y_xO_4$ (x = 0.00, 0.02, 0.04, 0.06, 0.08 and 0.10)

3.4 Dielectric and Impedance Formalism

3.4.1 Frequency-dependent Studies

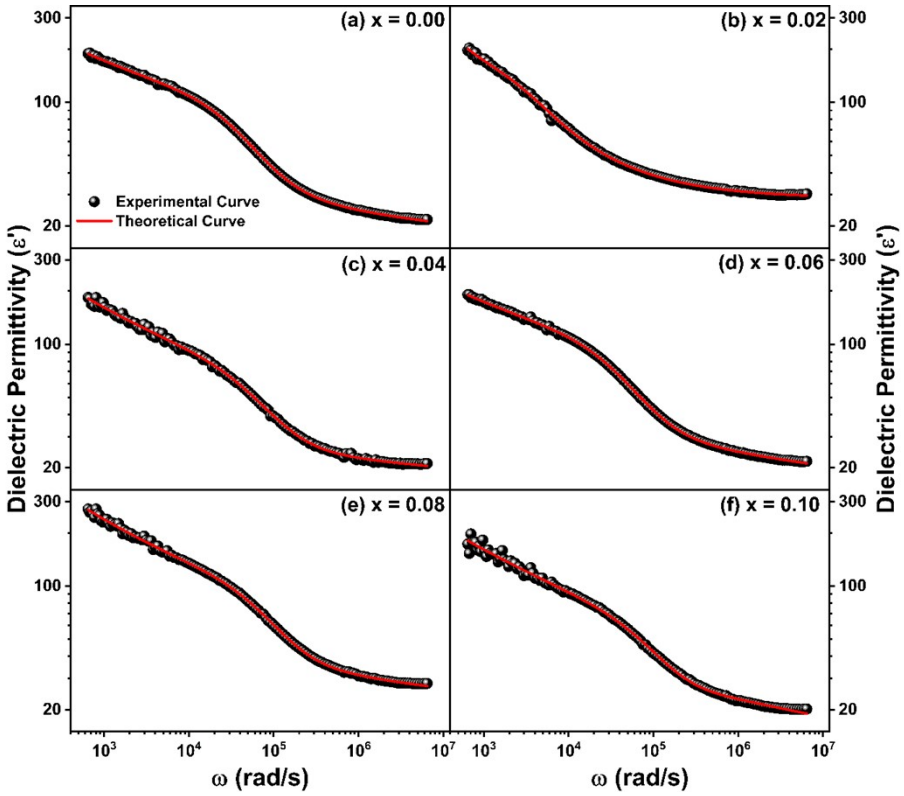

Figure S12. Theoretical fit using modified Havriliak Negami relaxation model associated with the conductivity of $CoFe_{2-x}Y_xO_4$

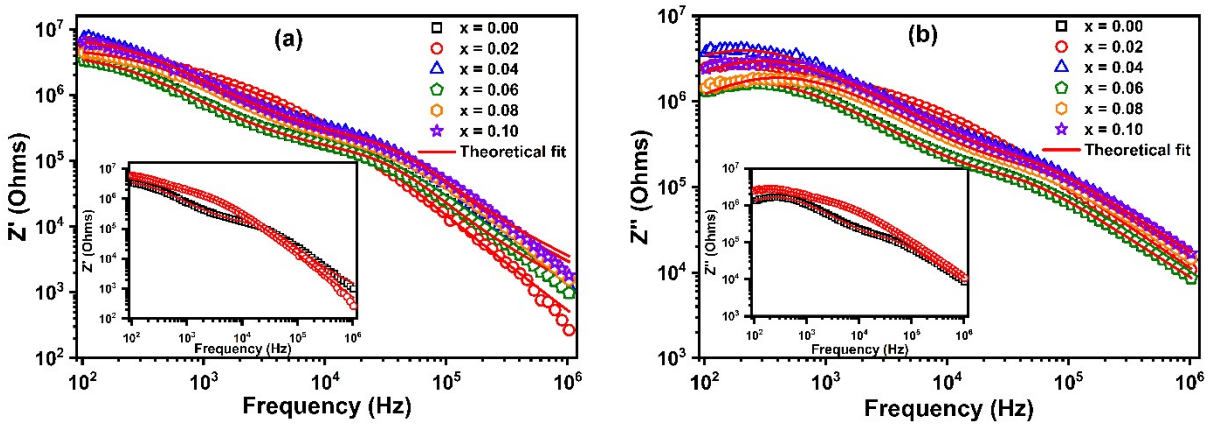

Figure S13. (a) variation of real impedance and (b) variations of the imaginary impedance of the $CoFe_{2-x}Y_xO_4$ system

Table S4. Variations of resistance, capacitance, and n value of grain and grain boundaries in $CoFe_{2-x}Y_xO_4$ system

x	R_g (MΩ)	C_g (pF)	R_{gb} (MΩ)	Q_{gb} (pF/Ω)	n_{gb}	C_{gb} (pF)	Q_{il} (pF/Ω)	n_{il}
0.00	0.11	38.47	4.39	552.44	0.82	147.3	-	-
0.02	1.62	378.90	13.68	13501.00	0.35	613.57	16.25	0.99
0.04	0.21	21.84	10.47	256.8	0.82	70.04	-	-
0.06	0.11	38.45	4.37	559.11	0.82	149.32	-	-
0.08	0.14	23.491	5.12	332.5	0.81	74.52	-	-
0.10	0.16	22.711	8.00	278.87	0.81	66.6	-	-

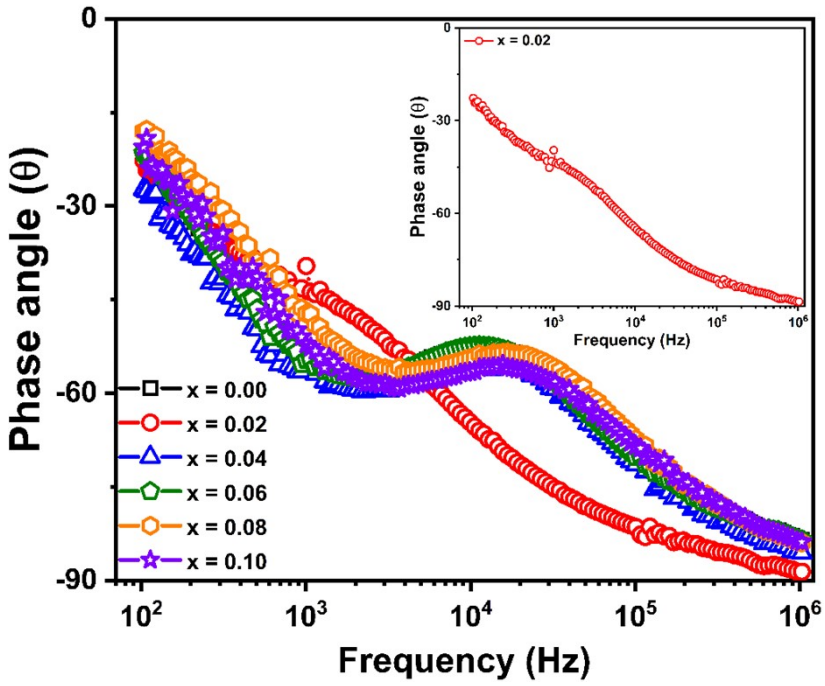

Figure S14. Phase angle variations of the $CoFe_{2-x}Y_xO_4$ system

3.4.2 Temperature-dependent studies

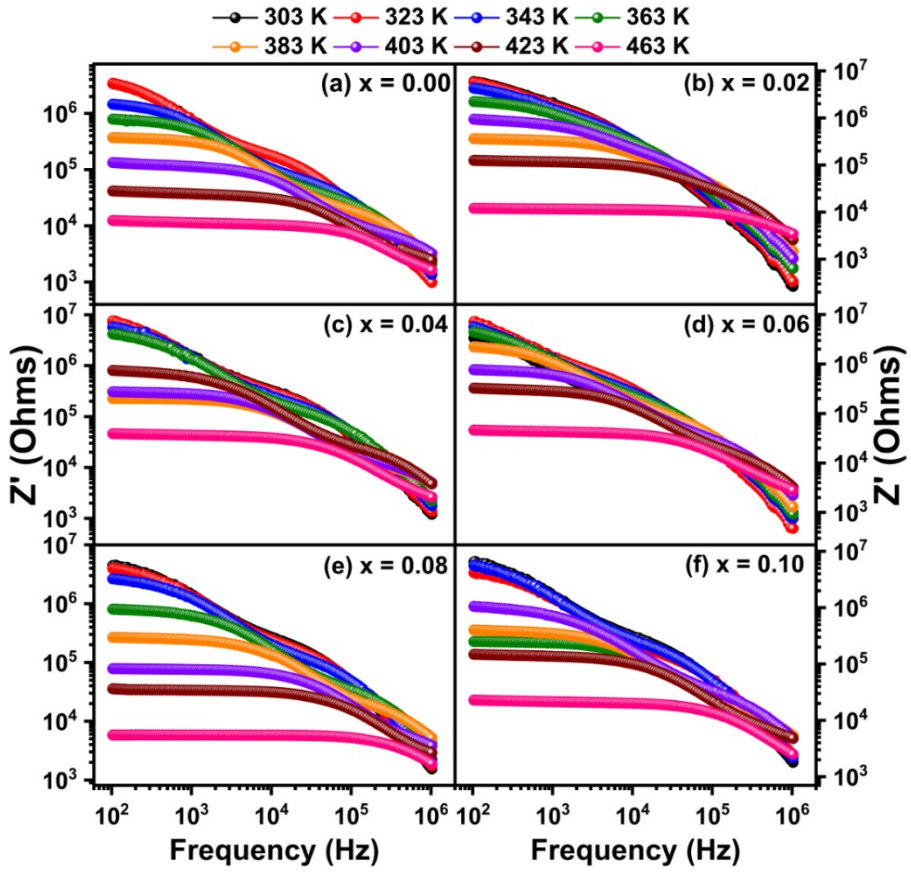

Figure S15. Temperature-dependent real impedance dispersion curve of $CoFe_{2-x}Y_xO_4$ system

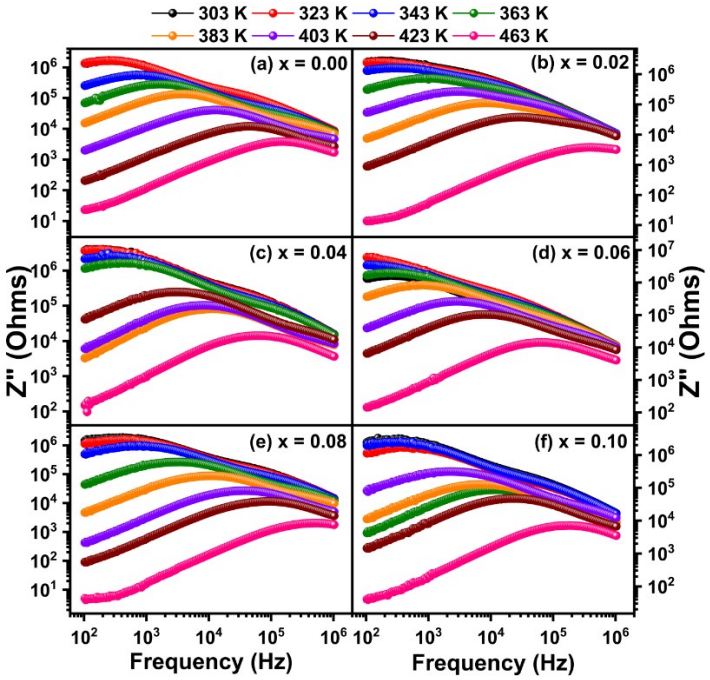

Figure S16. Temperature-dependent imaginary impedance dispersion curve of $CoFe_{2-x}Y_xO_4$ system

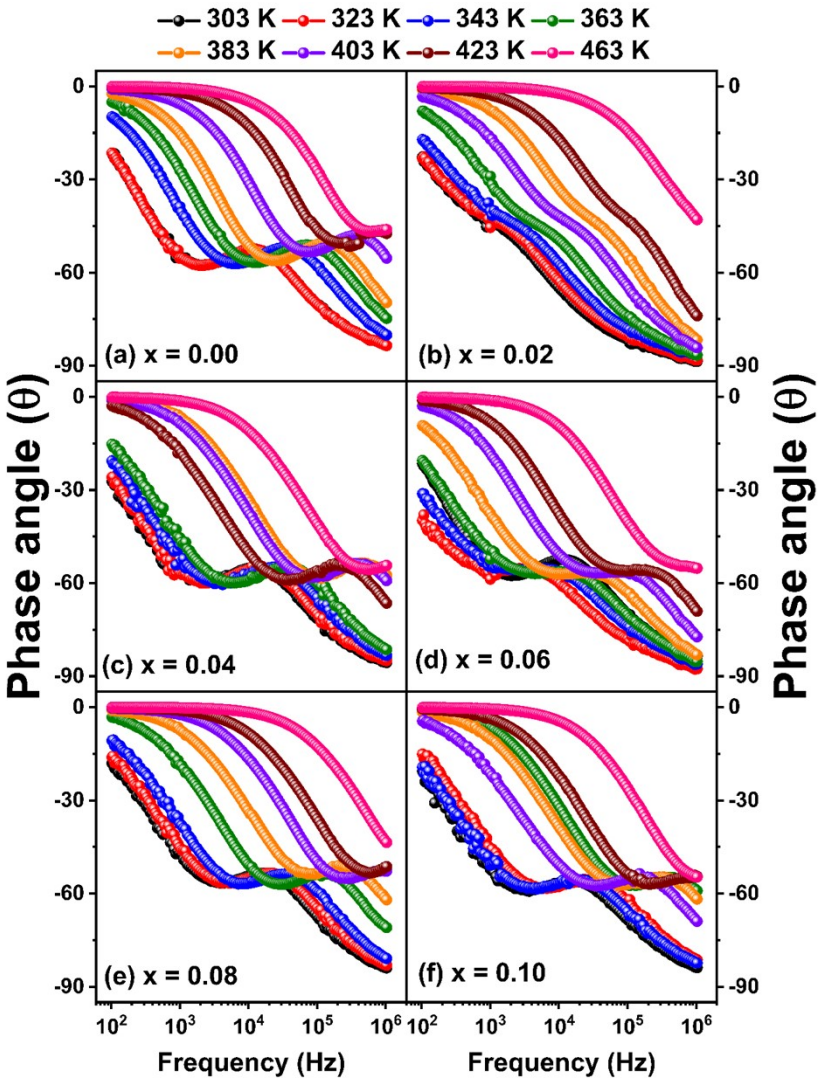

Figure S17. Temperature-dependent phase angle dispersion curve of $CoFe_{2-x}Y_xO_4$ system

3.5 A.C. conductivity studies

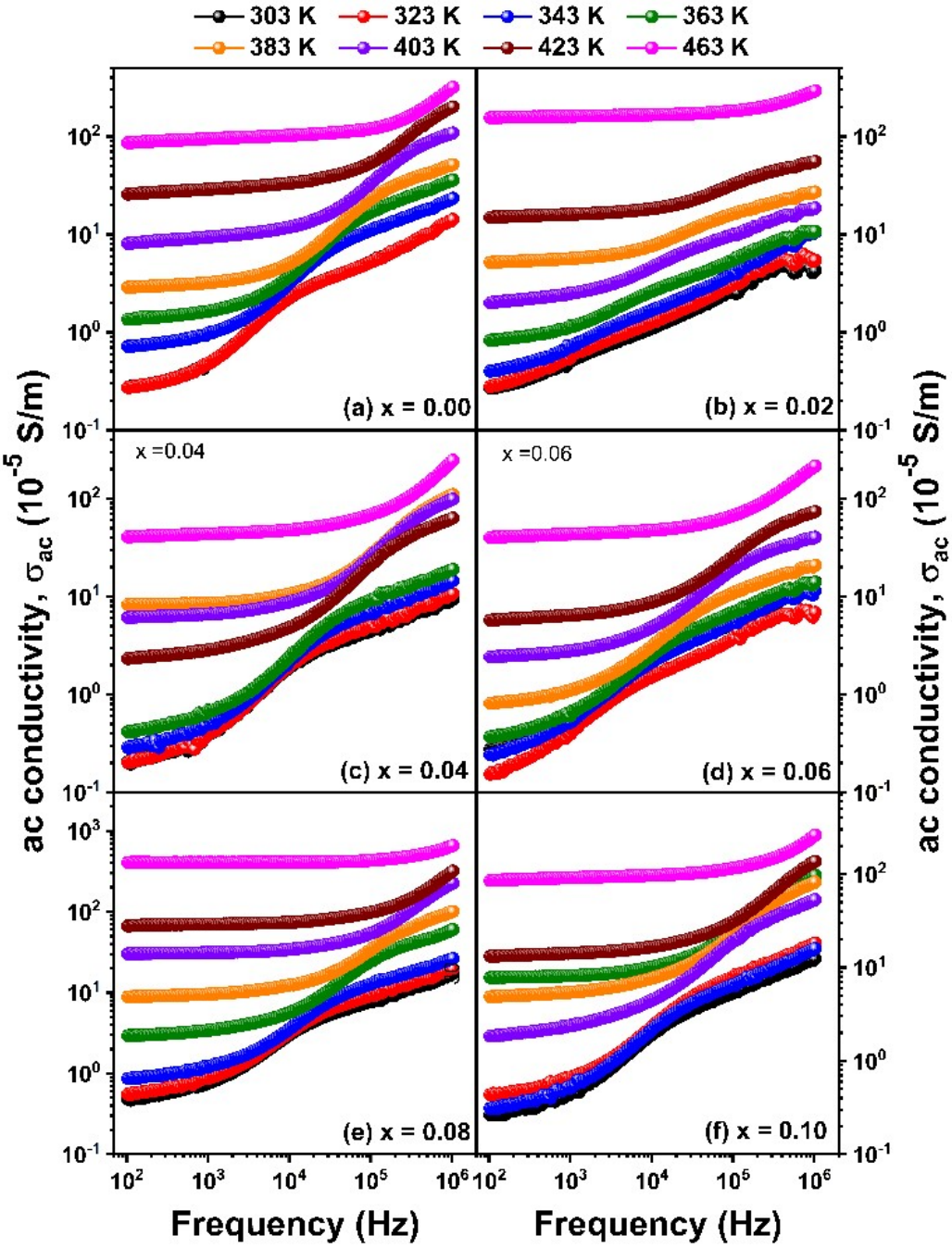

Figure S18. Temperature-dependent frequency response AC conductivity curve of $CoFe_{2-x}Y_xO_4$ system

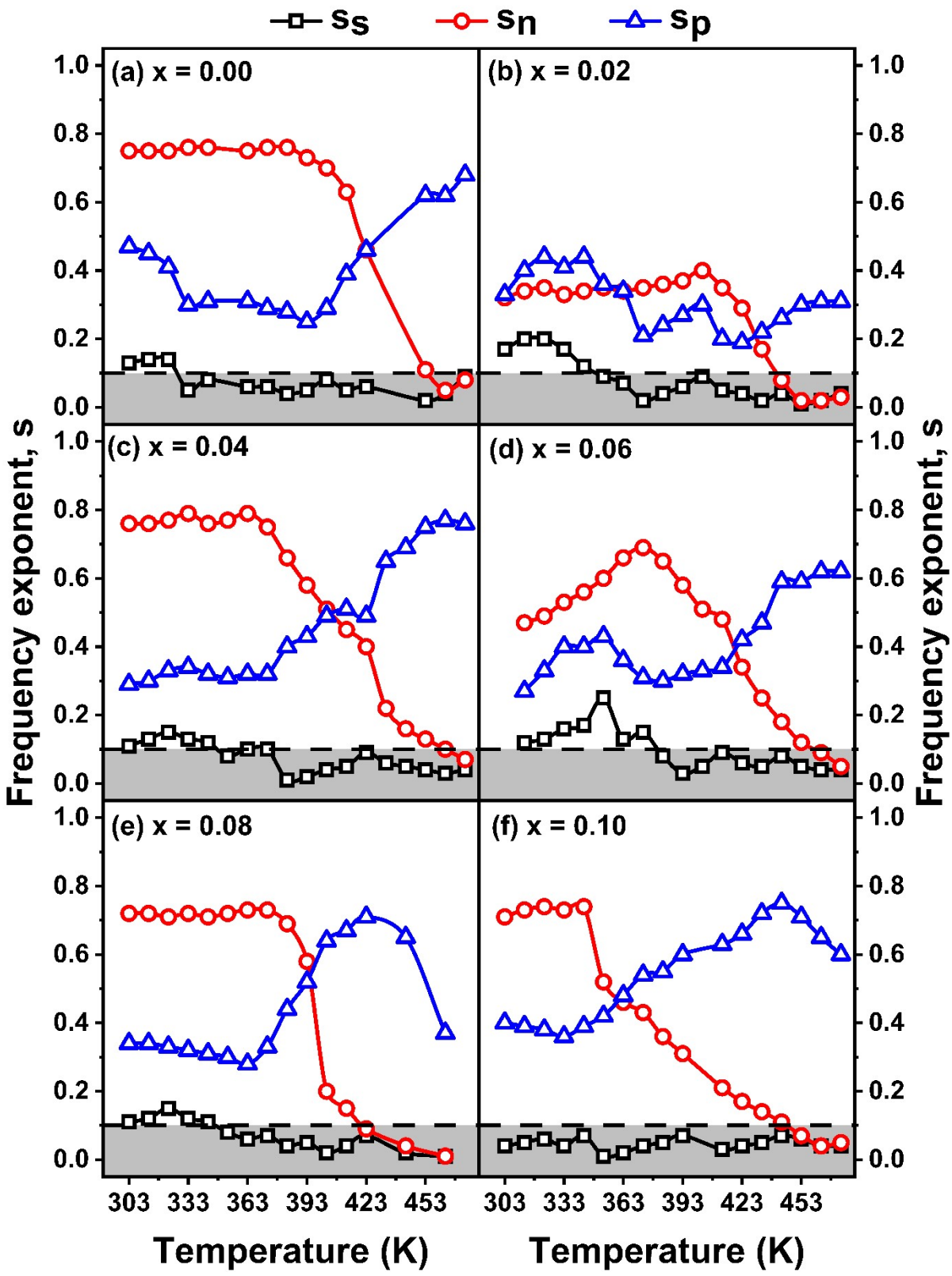

Figure S19. Variations of frequency exponent of different charge carriers of $CoFe_{2-x}Y_xO_4$ system with respect to temperature

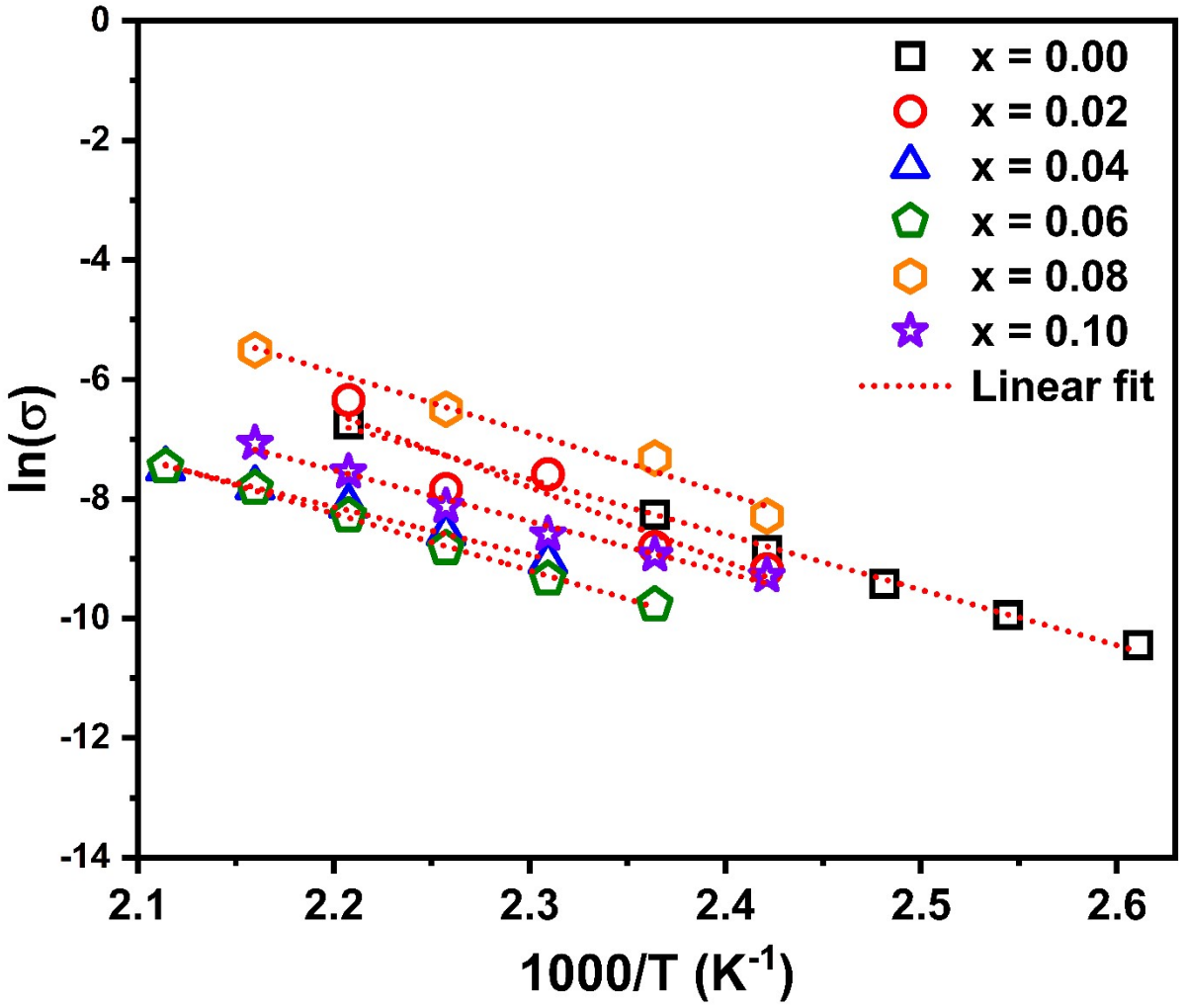

Figure S20. Estimation of activation energy (E_a) of $CoFe_{2-x}Y_xO_4$ (x = 0.00, 0.02, 0.04, 0.06, 0.08 and 0.10)

Table S5. Activation energy of $CoFe_{2-x}Y_xO_4$ system

Composition, x	Activation Energy (eV)
0.00	0.80
0.02	1.07
0.04	0.69
0.06	0.82
0.08	0.87
0.10	0.74